JMEPEG (2019) 28:4443–4453
https://doi.org/10.1007/s11665-019-04161-5

1059-9495/$19.00

Butt Laser Welding–Brazing of AZ31 Mg to Nickel-Coated Ti-6Al-4V

Laijun Wu, Jia Yang, Chengwei Zang, Caiwang Tan, Zequn Zhang, Xiaoye Zhao, Bo Chen, and Xiaoguo Song

(Submitted October 1, 2018; in revised form February 27, 2019; published online June 24, 2019)

Mg and Ti alloy are hard to be bonded due to their huge discrepancy in physical and metallurgical characteristics. As an intermediate element, Ni is feasible for joining of Mg and Ti. The interfacial microstructure and mechanical properties of laser-welded–brazed AZ31 Mg/Ti-6Al-4V joints in butt configuration were investigated with different thicknesses of electrodeposited Ni interlayer. The interfacial reaction products evolved from an ultra-thin Ti_3Al layer to Ti_2Ni layer mingled with Ti_3Al, and more Mg_3AlNi_2 compounds were produced in the fusion zone (FZ) as Ni coating thickness increased. Slag inclusions and cracks were observed in interfacial layer when coating thickness exceeded 2.5 μm. The quantity of Mg_3AlNi_2 and the thickness of interfacial layer decreased from the top to bottom of groove of the same joint owing to high thermal gradient during laser welding. The chemical potential of Al and Ni indicated that Al-Ti reaction product was produced more easily than Ni-Ti in 0.001Mg-(Ni-Al-Ti) system. The thermodynamic calculation results of Gibbs free energy suggested the preferential formation Ti-Al phase and Ti-Ni phase along the interface while the Mg-Al-Ni ternary phase in the FZ. Fracture loads of joints increased first followed by a decline with the increase in coating thickness. The joint fractured at the Mg base metal, reaching a maximum value of 3900 N with the Ni coating thickness of 1.5 μm. In the case of using thinner or thicker Ni coating, crack propagated along the interface due to the insufficient metallurgical bonding or defects existed in the interfacial layer. The characteristic of fracture surface changed from the tear ridges and terraces to river pattern when interfacial failure occurred.

Keywords laser welding–brazing, magnesium alloy, microstructure, Ni coating thickness, titanium alloy

1. Introduction

Recently, energy conservation has received explosive attention with the development of automobile and aerospace industry. The assembly of lightweight structural metal has great value in many fields due to its advantages over energy consumption and weight reduction (Ref 1). Dissimilar light alloy combination is an important way to realize lightweight structure, such as Al/Cu (Ref 2, 3), Al/steel (Ref 4-6), Mg/steel (Ref 7), Ti/Al (Ref 8-10), and Mg/Al (Ref 11). As the demand for lightweight alloy increases, magnesium (Mg) and its alloys have gained popularity in industrial applications owing to prominent properties such as recyclability, high specific strength and low density (Ref 12, 13). Ti-6Al-4V alloy is widely used in the aerospace and defense industries because of the high specific strength and corrosion resistance (Ref 14, 15). Therefore, achieving a reliable bonding of Mg and Ti is of great significance in expanding the utilization of both alloys.

Laijun Wu, Jia Yang, Chengwei Zang, Xiaoye Zhao, and **Bo Chen**, State Key Laboratory of Advanced Welding and Joining, Harbin Institute of Technology, Harbin 150001, China; and **Caiwang Tan, Zequn Zhang,** and **Xiaoguo Song**, State Key Laboratory of Advanced Welding and Joining, Harbin Institute of Technology, Harbin 150001, China; and Shandong Provincial Key Laboratory of Special Welding Technology, Harbin Institute of Technology at Weihai, Weihai 264209, China. Contact e-mail: tancaiwang@hitwh.edu.cn.

However, there are some challenges in direct joining of Mg to Ti due to their huge discrepancy in physical and metallurgical characteristics. The melting point of Mg is 649 °C while that of Ti is 1678 °C, and the boiling point of Mg is 1091 °C. The conventional fusion welding process is unsuitable because Mg would vaporize when Ti melt. Furthermore, it is difficult to produce atomic diffusion or reaction layer due to the immiscibility characteristics of Mg and Ti. Hence, a feasible process using an intermediate element which can react with both Mg and Ti is vital to achieve metallurgical bonding at the interface.

The established methods to achieve metallurgical bonding by intermediate element could be mainly summarized in two ways: mutual diffusion of alloying elements from filler metals or base metals (Ref 16-19) and adding interlayer elements (Ref 20). In the friction stir welding (FSW) process (Ref 16), the Mg-Al-Zn alloys and Ti dissimilar butt joints were achieved due to the diffusion of Al element from base metal. The metallurgical bonding was successfully realized by Al-rich thin layers and Ti-Al intermetallic layers formed at the interface. Gao et al. (Ref 17) performed laser keyhole welding of thicker Mg and Ti. The interfacial reaction occurred in the Ti-weld interfacial layer, and the reaction product was identified as $Mg_{17}Al_{12}$. Cao et al. (Ref 18) employed Al element from AZ61 Mg-based filler to improve Mg/Ti bonding by cold metal transfer welding–brazing (CMT) process. Ti_3Al phase newly formed at the brazing interface, indicating that Al element was crucial to realize metallurgical bonding between Mg and Ti base metals. Tan et al. (Ref 19) employed AZ92 Mg-based filler containing 9 wt.% Al element to bond Mg and Ti using laser welding–brazing process. A rather thin reaction layer formed at the brazing interface, which was identified as Ti_3Al phase. In the case of adding interlayer, the approach was usually achieved by adding foil (Ref 20-22) or electro-coated layer

(Ref 23-25). Ni interlayer was employed to join Ti-6Al-4V and Mg-AZ31 alloys in the TLP joining process (Ref 20). Eutectic formed at Mg–Ni interface and solid-state diffusion occurred at Ni–Ti interface, respectively. In our previous study, Al foil (Ref 21, 22), copper coating (Ref 23) and Ni coating (Ref 24, 25) were successfully employed to achieve laser welding–brazing of Mg to Ti. Sound joints were obtained by Ni coating and the Ni electro-coated layer improved wetting–spreading ability of molten Mg on Ti substrate. The laser power had a great impact on mechanical properties and microstructure. However, it should be noticed that thickness of the interlayer determined the thickness and morphology of the reaction layer directly, which was worth investigating in detail.

Therefore, the objective of the current work is to investigate the influence of Ni coating thickness on laser lap welding–brazing of Mg to Ti, including weld appearance, interfacial microstructure and mechanical properties. The thermodynamic analysis was conducted to illustrate the bonding mechanism of Mg-/Ni-coated Ti joints.

2. Experimental Procedure

2.1 Materials and Electrodeposition Process

A 1.5-mm-thick AZ31B magnesium alloy with 2.5-3.5 wt.% Al and 1.0-mm-thick Ti-6Al-4V titanium alloy with 5.5-6.8 wt.% Al were employed as base metals in the present study. All plates were prepared with the dimension of 100 mm long and 50 mm wide. The welding wire used was 1.6-mm-diameter AZ92 Mg-based filler with 8.3-9.7 wt.% Al. In order to remove the surface oxides, 80% distiller, 5% HF and 15% HCl were blended to soak Ti sheets before electroplating. After cleaned by running water, Ti sheet was put into electroplating solution as the cathode. The composition of electroplating solution is listed in Table 1. The speed of magnetic stirrer, temperature and electric current during process was kept at 250 r/min, 25 °C and 0.3 A, respectively. Uniform Ni coating was observed on Ti sheet with different coating time as shown in Fig. 1(a)-(e). Coating time was set as a function of coating thickness, and the results obtained in this work are plotted in Fig. 1(f).

2.2 Laser Welding–Brazing Process

Figure 2 shows the schematic illustration of laser welding–brazing process. The Ti sheet with a 45-angle groove and Mg sheet were both cleaned by acetone before clamping. The butt configuration with the bottom gap of 0.3 mm was adopted. Fiber laser (IPG YLR-6000) was used, and main technical parameters are exhibited in Table 2. Argon used as a shielding gas to protect metals from oxidation during welding. Its flow was kept at 10 L/min. The backing plate was Cu which was good for heat dissipation. The laser beam was focused on the spot about +20 mm away from Ti surface, which was localized in the filler. The filler was fed at a speed of 3 m/min ahead of laser beam. The laser power and welding speed were set as 1500 W and 0.5 m/min, respectively.

2.3 Analysis Methods

The laser-welded–brazed joints were then cut along the vertical direction of weld seam with the size of 15 mm long × 7 mm wide. Standard metallographic preparation procedure was performed. The cross sections were observed by optical microscope. Scanning electron microscope (SEM) equipped with energy-dispersive spectrometer (EDS) was utilized to analyze the evolution of microstructure and identify the reaction products. Samples with length of 80 mm and width of 10 mm were prepared for tensile shear testing which was carried out with the crosshead speed of 0.5 mm/min at room temperature.

2.4 Thermodynamic Analysis

The chemical potential of Mg, Ti, Ni and Al was calculated based on the Miedema model and Toop model which was extended from Miedema theory (Ref 26). The corresponding theoretical interpretations were given as follows: (1)

$$\begin{aligned}\Delta G^E = {} & \frac{x_2}{1-x_1}\Delta G^E_{12}(x_1;1-x_1)+\frac{x_3}{1-x_1}\Delta G^E_{13}(x_1;1-x_1)\\ & +\frac{x_4}{1-x_1}\Delta G^E_{14}(x_1;1-x_1)\\ & +(x_2+x_3)^2\Delta G^E_{23}\left(\frac{x_2}{x_2+x_3};\frac{x_3}{x_2+x_3}\right)\\ & +(x_2+x_4)^2\Delta G^E_{24}\left(\frac{x_2}{x_2+x_4};\frac{x_4}{x_2+x_4}\right)\\ & +(x_3+x_4)^2\Delta G^E_{34}\left(\frac{x_3}{x_3+x_4};\frac{x_4}{x_3+x_4}\right)\end{aligned} \quad \text{(Eq 1)}$$

$$G_m = G^{\mathrm{ID}} + G^E \quad \text{(Eq 2)}$$

$$\mu_i = \frac{\partial G_m}{\partial x_i} \quad \text{(Eq 3)}$$

where ΔG^E was the excessive Gibbs energy for quaternary and binary systems, x_i was the mole fraction of components in the system, μ_i was the chemical potential of components, G^{ID} was the Gibbs free energy of ideal solution approximation. The excess Gibbs energy of binary system could be calculated by the mixing enthalpy. According to the Miedema theory, the mixing enthalpy of binary alloys could be expressed as:

$$\Delta H_{1,2} = f_{1,2}\frac{x_1[1+\mu_1 x_2(\varphi_1-\varphi_2)x_2[1+\mu_2 x_1(\varphi_2-\varphi_1)}{x_1 V_1^{2/3}[1+\mu_1 x_2(\varphi_1-\varphi_2)]+x_2 V_2^{2/3}[1+\mu_2 x_1(\varphi_2-\varphi_1)]} \quad \text{(Eq 4)}$$

Table 1 The Ni electroplating solution composition (g/L)

Composition	$CuSO_4{\cdot}6H_2O$	NaCl	H_3BO_3	Na_2SO_4	$MgSO_4{\cdot}7H_2O$
Value	200	10	32	70	60

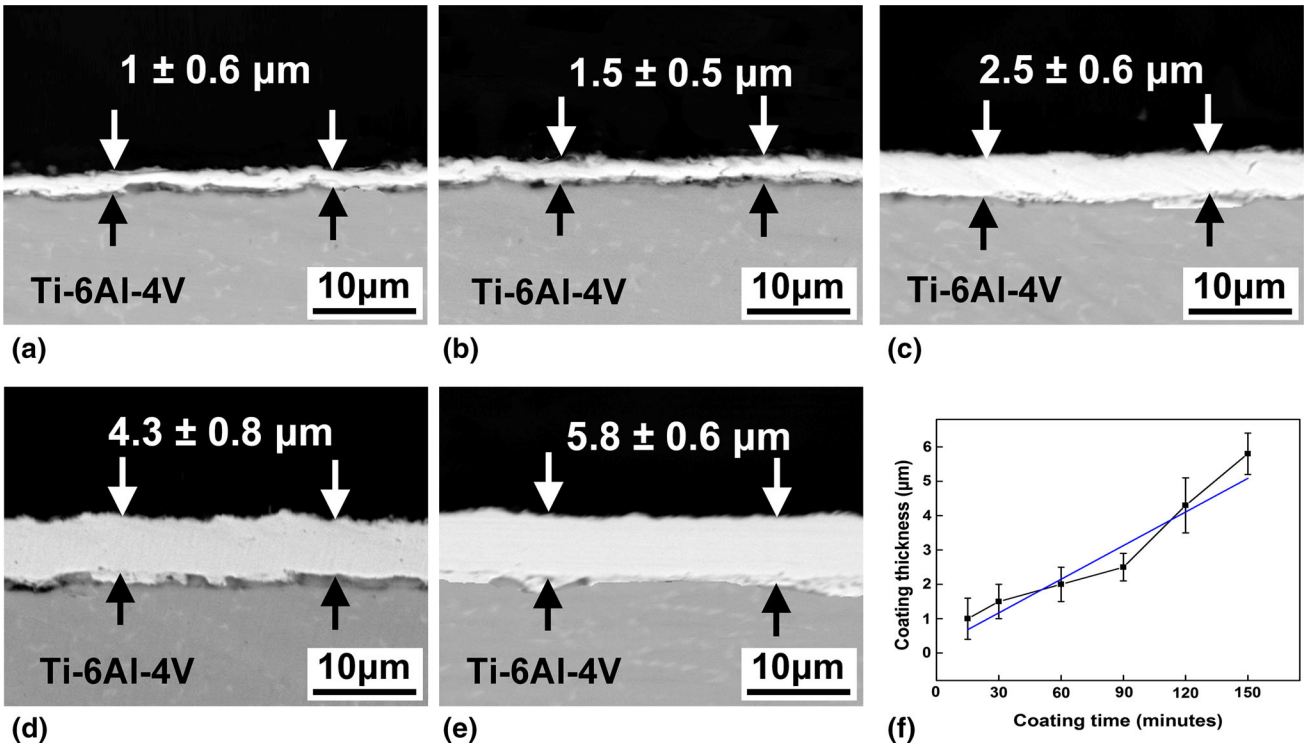

Fig. 1 Micrograph of Ni coating on Ti surface with different coating time: (a) 15 min; (b) 30 min; (c) 90 min; (d) 129 min; (e) 150 min; (f) effect of electroplating time on coating thickness

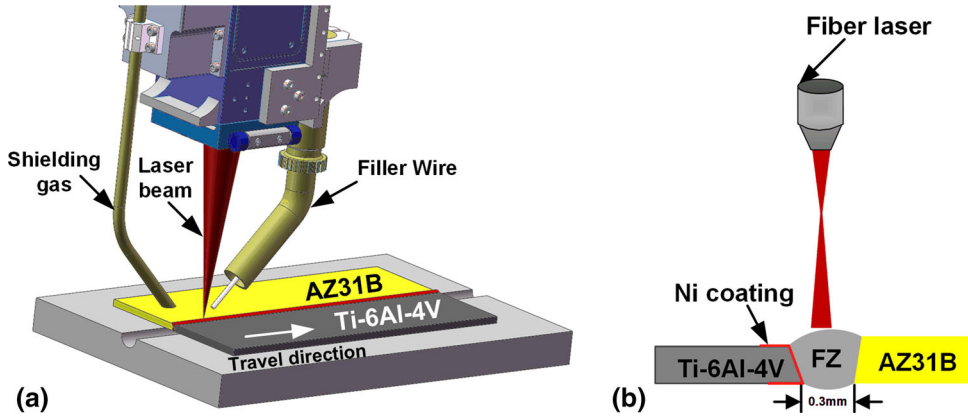

Fig. 2 Schematic illustration of laser welding–brazing Mg-/Ni-coated Ti in butt configuration: (a) The configuration before welding; (b) welding process

Table 2 The main technical parameters of fiber laser

Maximum power, kW	6
Beam parameter product, mm × mrad	8
Wavelength, nm	1070
Diameter of focused laser beam, mm	0.2

$$f_{1,2} = \frac{2pV_1^{2/3}V_2^{2/3}\left[q/p\left(\Delta n_{\mathrm{WS}}^{1/3}\right)^2 - (\Delta\varphi)^2 - a(r/p)\right]}{(\Delta n_{\mathrm{WS}}^{1/3})_1^{-1} + (\Delta n_{\mathrm{WS}}^{1/3})_2^{-1}} \quad \text{(Eq 5)}$$

Table 3 Parameters adopted of Mg, Ti, Al, Ni elements (Ref 26)

Element	T_m, K	n_{ws}, d.u.	φ, V	μ	V, cm^3	R/P
Mg	922	1.6	3.45	0.1	14	0.4
Ti	1933	3.51	3.8	0.04	10.58	1
Al	933.6	2.7	4.2	0.07	10.58	1
Ni	1726	5.36	5.26	0.04	6.6	1

$$G_{12}^E = \Delta H_{1,2}\left[1 - \frac{T\left(\frac{1}{T_{m,i}} + \frac{1}{T_{m,j}}\right)}{14}\right] \quad \text{(Eq 6)}$$

where $f_{1,2}$ indicated the influence of one element to another, $\emptyset$ was electronegativity, V was molar volume, Δn_{WS} was electron concentration and q, r, μ, a were the empirical parameters. The parameters adopted of Mg, Ti, Al, Ni elements are as shown in Table 3 (Ref 26). G_{ij}^{E} was acquired based on Tanaka's theory (Ref 6). The chemical potential was the partial molar free energy calculated based on the above formulas.

3. Results and Discussion

3.1 Joint Appearance and Cross Section

Figure 3 shows typical appearances and cross sections of Mg/Ti joints with various Ni coating thicknesses. Smooth and uniform appearances (Fig. 3(a1)-(d1)) were obtained, which was related to the addition of Ni coating. Our previous studies have proved that liquid Mg-based filler exhibited better wetting and spreading performance on Ni-coated Ti than on bare Ti (Ref 21, 22). The corresponding cross sections indicated some differences with the increase in Ni coating thicknesses. The contact angle of joint decreased from 60.3° to 36.3° when coating thickness increased from 1 to 1.5 μm, as shown in Fig. 3(a2) and (b2). However, bigger wetting angles were observed with thicker Ni coating thickness in Fig. 3(c2) and (d2). It was mainly because the reaction layer at groove surface (white arrows in Fig. 3(d2)) or unmelted coating on Ti upper surface restrained the wetting and spreading of molten Mg filler metal. The fluctuation of laser welding–brazing process resulted in the slight variation of contact angle in Fig. 3(c2) and (d2).

3.2 Interfacial Microstructure of Mg-/Ni-Coated Ti Joint

Figure 4 shows the evolution of Mg/Ti joint microstructures with various Ni coating thickness. High-temperature gradient induced by the laser welding–brazing process contributed to varied SEM morphologies at the different zones along the groove interface. Thus, the joint interfaces from top to bottom regions were observed, respectively. EDS analysis results of typical phases are listed in Table 4.

Figure 4(a1)-(a3) shows the microstructure morphology of Mg/Ti interface bonded with Ni coating thickness of 1 μm. In the FZ of top region (Fig. 4(a1)), some tiny blocked phases P2 and strip-shaped microstructures P3 were distributed in the dark matrix P1. The EDS analysis result confirmed P1 was α-Mg. P2 was composed of 22.90 at.% Al, 60.29 at.% Mg and 16.81 at.% Ni, which was identified as Mg-Al-Ni ternary intermetallic compound. This occurred as Ni coating melted and was

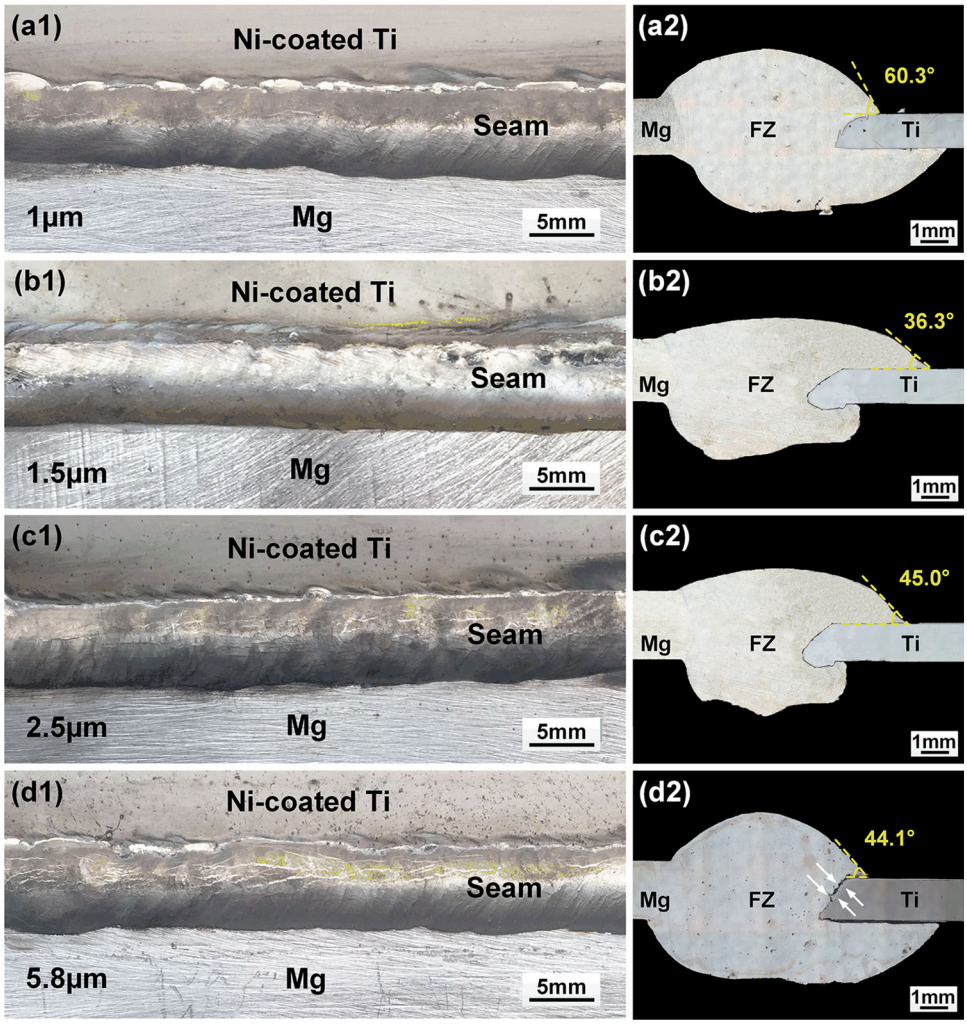

Fig. 3 Joint appearances and cross sections with various Ni coating thicknesses: (a) 1 μm; (b) 1.5 μm; (c) 2.5 μm; (d) 5.8 μm

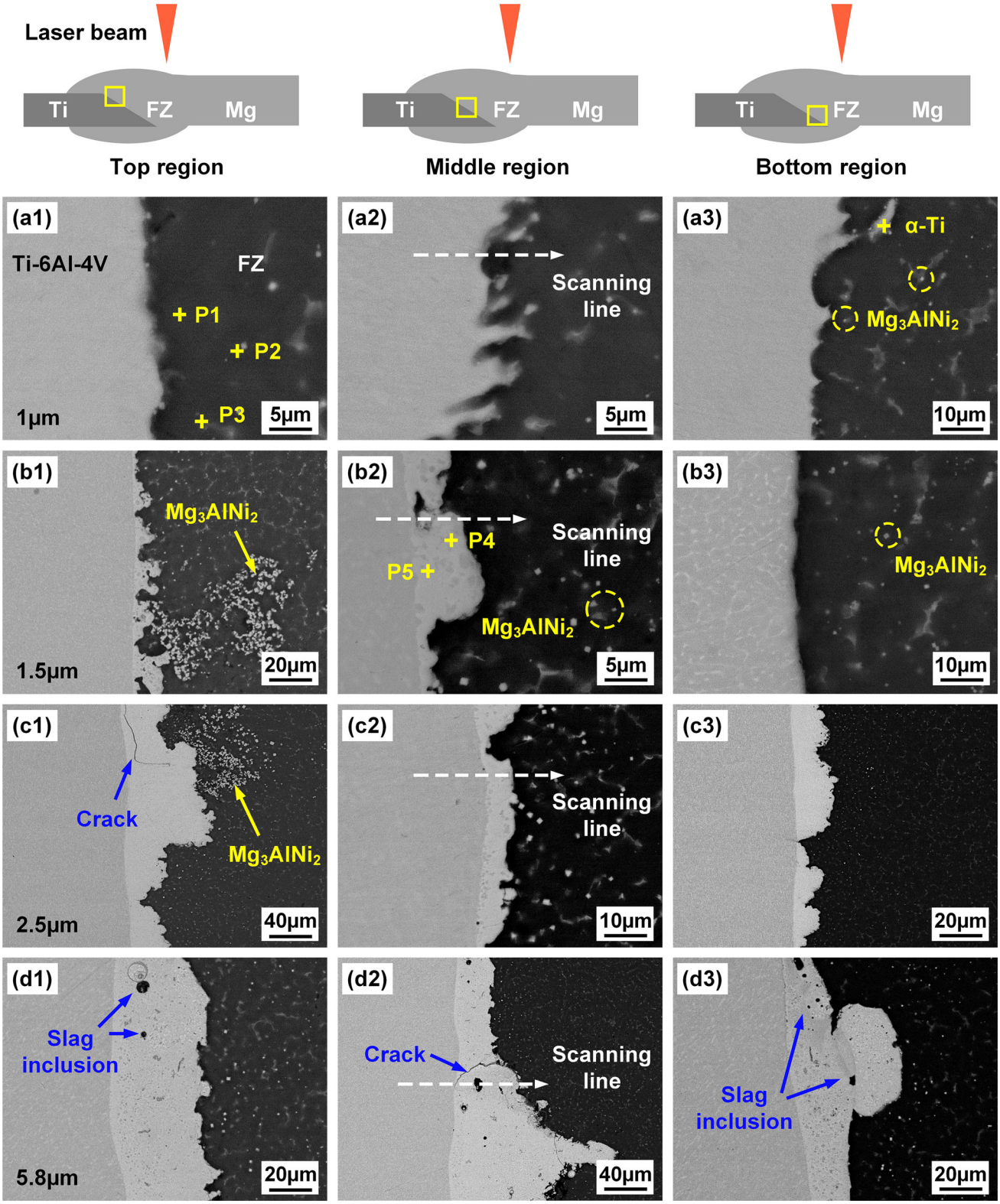

Fig. 4 SEM microstructures of Mg-/Ni-coated Ti with various coating thickness at different regions: (a1)-(a3) 1 μm; (b1)-(b3) 1.5 μm; (c1)-(c3) 2.5 μm; (d1)-(d3) 5.8 μm

involved in the FZ adjacent to Ti interface, which was then reacted with Al and Mg atoms. These blocked phases were also reported in our previous study (Ref 25), in which Mg- and Ni-coated Ti was bonded in lap configuration using the same welding technique. Tan et al. identified that this Mg-Al-Ni ternary phase was Mg_3AlNi_2 compound. Based on EDS result, P3 was confirmed as $Mg_{17}(Al, Zn)_{12}$, which was commonly observed in weld joint of Mg/Ti alloy.

As for the interface, no obvious reaction layer was observed at all three regions in Fig. 4(a1)-(a3). The EDS line scanning

was conducted to detect element fluctuation across the interface of middle region, and the result is plotted in Fig. 5(a). Al element peaked and no Ni element concentrated, which indicated interfacial layer containing Al without any Ni was produced. Thin Ni coating was totally involved in the molten pool under the action of flow and stirring, which was responsible for no Ni enrichment. Based on Al-to-Ti atomic ratio, Al to Ti was one to three, and thus Ti_3Al interfacial phase was confirmed. In the research of Mg/Ti joint (Ref 19), Ti_3Al layer was considered as a crucial reaction product in achieving metallurgical bonding. Therefore, it was inferred that the joining between Mg alloy and Ti alloy mainly depended on this Ti-Al interfacial layer when Ni coating was thin in this study.

Table 4 Component of different points in Fig. 4 (at.%)

Point	Mg	Al	Ti	Ni	Zn	Possible phase
P1	96.05	3.75				α-Mg
P2	60.29	22.90		16.81		Mg_3AlNi_2
P3	80.49	2.94			2.94	$Mg_{17}(Al,Zn)_{12}$
P4		24.63	61.56	13.81		Ti_3Al
P5		21.49	55.44	23.07		Ti_2Ni

With the increase in Ni coating thickness to 1.5 μm (Fig. 4(b1)-(b3)), the microstructure morphologies presented distinct difference from the former case. A large amount of Mg_3AlNi_2 was observed in the FZ of top region as shown in Fig. 4(b1). An obvious and inhomogeneous layer was produced along the interface of middle region and bottom region (Fig. 4(b2) and (b3)). Thicker Ni coating thickness offered more Ni atoms participating in reaction with Mg, Al or Ti atoms, which was the reason for the increase in Mg-Al-Ni ternary phase and interfacial layer. Note that the quantity of Mg_3AlNi_2 and the thickness of interfacial layer decreased from the top region to bottom region as presented in Fig. 4(b1)-(b2). This phenomenon was attributed to high thermal gradient owing to the local density laser energy along the Ti surface. Li et al. (Ref 27) found that reaction layer thickness was different in different regions of laser-welded–brazed Al/steel joints. The reaction layer thickness at the bottom was thicker than that at the bottom region. They proved the top interface acquired the highest temperature by employing numerical simulation. Figure 4(b2) clearly shows the reaction layer was composed of dark gray particles P4 and light gray matrix phase P5. P4 and

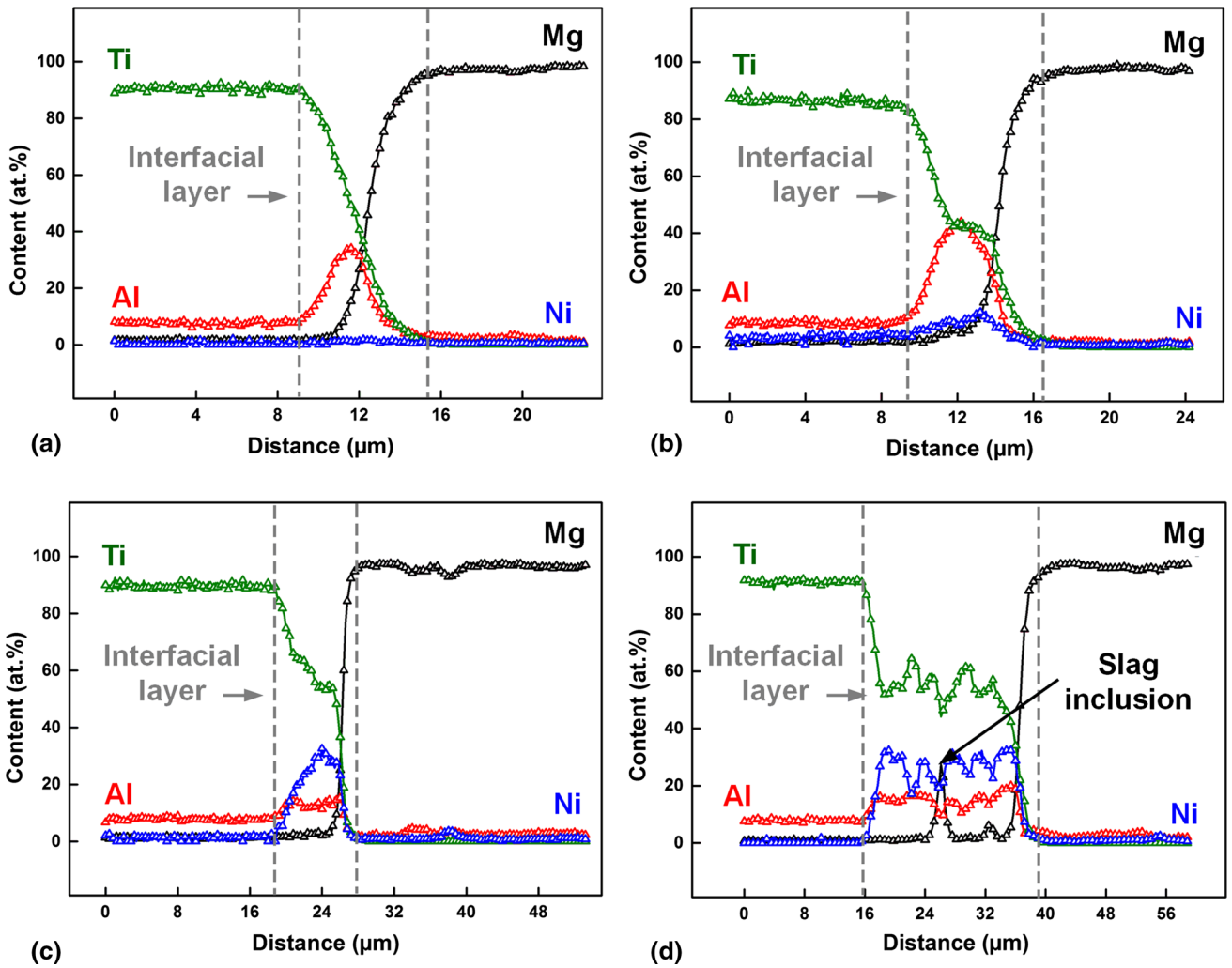

Fig. 5 Line scanning results of Mg-/Ni-coated Ti with various coating thickness at middle regions: (a) 1 μm; (b) 1.5 μm; (c) 2.5 μm; (d) 5.8 μm

P5 were ascertained as Ti_3Al and Ti_2Ni for their elemental composition containing 24.63 at.% Al, 61.56 at.% Ti, 13.81 at.% Ni and 21.49 at.% Al, 55.44 at.% Ti, 23.07 at.% Ni, respectively. The relevant line scanning result (Fig. 5(b1)) verified that Ni and Al element concentrated at the interface, which was in accordance with the formation of Ti_2Ni+Ti_3Al mixed reaction layer.

On the further increasing the Ni coating thickness to 2.5 μm (Fig. 4(c1)-(c3)) and 5.8 μm (Fig. 4(d1)-(d3)), the microstructure in the FZ exhibited similar characteristics with that shown in Fig. 4(b1)-(b3). The FZ consist of Mg_3AlNi_2 and $Mg_{17}Al_{12}$ compounds. The difference was the mixed interfacial reaction layer grew dramatically even at the bottom region. The EDS line scanning result shown in Fig. 5(c) and (d) suggested the concentration of Ni element and Al element occurred. A peak of Mg element occurred at interfacial layer in Fig. 5(d), which was attributed to slag inclusion produced during cooling stage. Additionally, it was worth noting that some cracks and slag inclusions generated in interfacial layer in Fig. 4(c1) and (d1)-(d3) when compared with Fig. 4(b1)-(b3), which would deteriorate joint strength. The presence of crack was closely associated with the great difference in thermal conductivity and thermal expansion coefficient between the Mg and Ti base metals. The thermal conductivity and thermal expansion coefficient of pure Mg were 145 Mm^{-1} k^{-1} and 25.8 × 10^{-6} k^{-1} while that of pure Ti were 12.56 Mm^{-1} k^{-1} and 9.24 × 10^{-6} k^{-1}, respectively. Therefore, welding stress was easily induced during the laser welding process characterized by rapid heating and cooling rate. In addition, Ti_2Ni was brittle IMC which had cracking trend under the effect of welding stress when its thickness exceeded a certain degree. The result was similar to the previous study that crack may easily form if the thickness of Fe-Al reaction layer reached 10 μm (Ref 27).

The EDS mapping result evidently showed the element distribution across the interface at middle region with the Ni coating thickness of 5.8 μm (Fig. 6). As presented, Ti and Al gathered in block form and Ni element peaked at the Ti side, revealing that blocked phase rich in Ti, Al and reaction layer containing Ti, Ni were produced along the interface. This observation confirmed the formation of Ti_3Al and Ti_2Ni, agreeing with the phase identification in Fig. 4(b2) and line scanning analysis in Fig. 5(d).

3.3 Interfacial Thermodynamic Analysis

The thermodynamic calculation results of formation enthalpy and chemical potential at the interface of FZ/Ti, as shown in Fig. 7. According to our previous work (Ref 24), the temperature was set as 1500 K for thermodynamic calculation. The results of the binary system formation enthalpy at 1500 K are shown in Fig. 7(a). The positive standard molar enthalpy of formation of Mg-Ti system suggested that spontaneous reaction between Mg and Ti was impossible. The Ni-Ti, Al-Ti, Ni-Al, Mg-Ni and Mg-Al compounds tended to form with negative formation enthalpies, which consist of the EDS results in Fig. 4 and Table 4. What's more, the standard molar enthalpies of Ni-Ti and Al-Ti were the lowest among these binary systems, indicating that the driving force was much higher for producing Ni-Ti and Al-Ti compounds.

The chemical potential of Al-Ti and Ni-Ti was further compared in Mg-Ni-Al-Ti quaternary system, and the thermodynamic calculation results are shown in Fig. 7(b) and (c). The content of Al was set as 0.101 (based on the content of 9 wt.% in AZ92 filler). As shown in the figure, the chemical potential gradient of Al was 94.009 kJ/mol and that of Ni was 74.537 kJ/mol, suggesting that there was a higher driving force of Al from fusion zone to Ti substrate than that of Ni, which explained why Ti-Al phase precipitated more easily than Ti-Ni phase (Fig. 4).

Figure 7(d) and (e) shows the Gibbs free energy of 0.001Mg-(Ni-Al-Ti) system and (Mg-Ni-Al)-0.047Ti system, respectively, with the position of minimum value marked by the

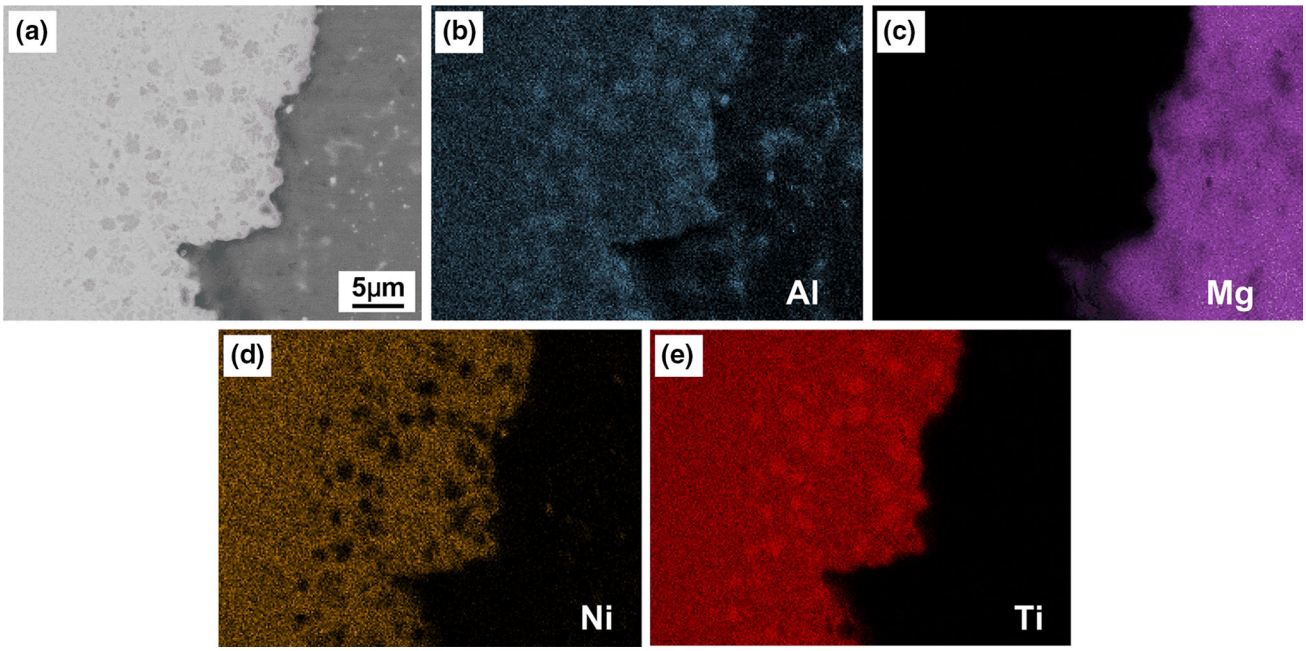

Fig. 6 Mapping scanning result at the middle region with the Ni coating thickness of 5.8 μm: (a) SEM morphology; (b-e) Al, Mg, Ni and Ti mapping

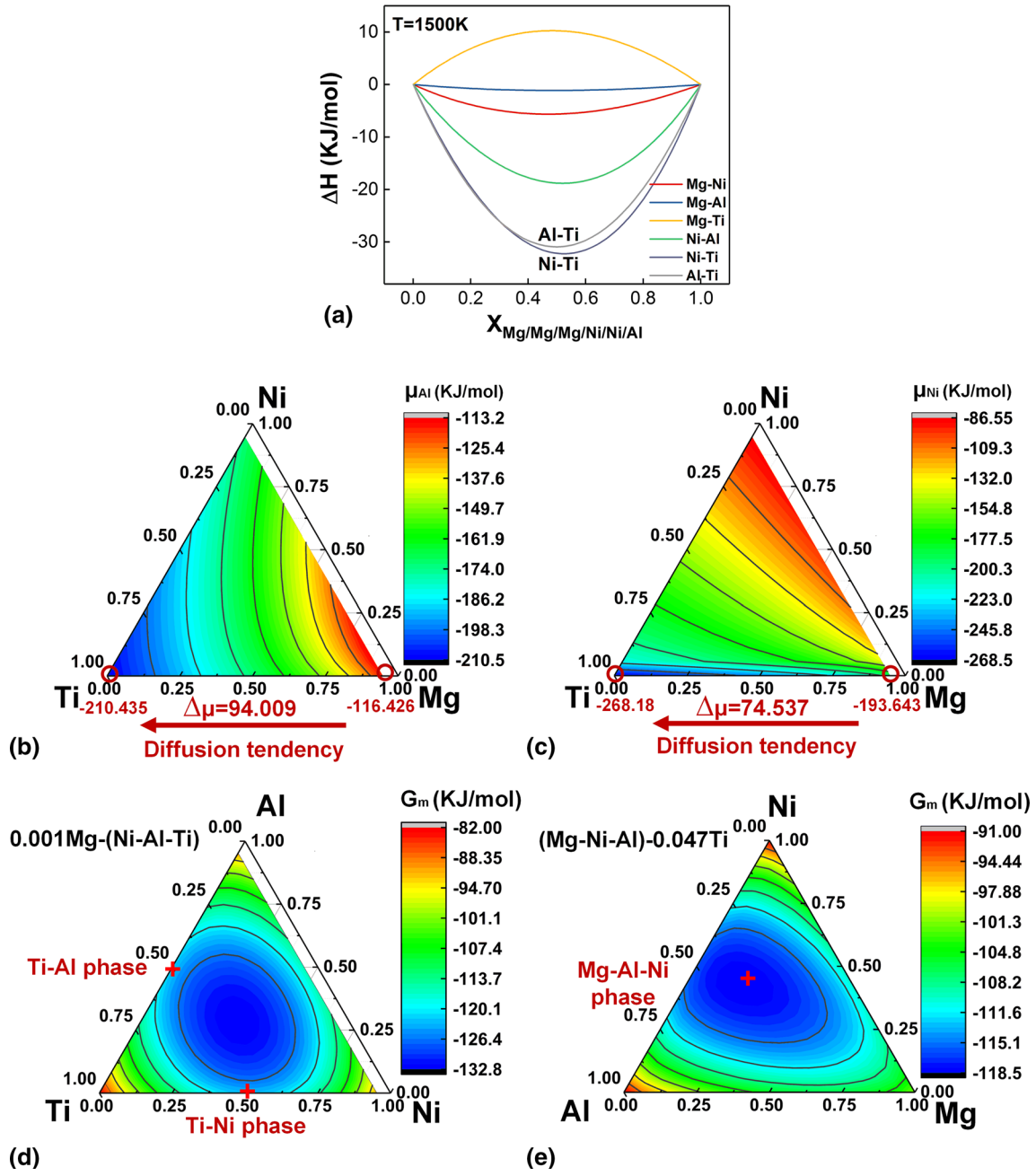

Fig. 7 Thermodynamic calculation results at 1500K: (a) formation enthalpy of binary systems; (b), (c) Chemical potential gradient of Al and Ni atoms; (d) Gibbs free energy of 0.001Mg-(Ni-Al-Ti) system;(e) Gibbs free energy of (Mg-Ni-Al)-0.047Ti system

red crosses. Mg barely existed and its content was set as 0.001 at the interface, similarly, the content of Ti in the FZ was quite low which was set as 0.047. It can be inferred that the formation of Ti-Al and Ti-Ni phases could be deduced for the minimum Gibbs free energy along the interface as shown in Fig. 7(d). In the same way, the Gibbs free energy shown in Fig. 7(e) indicated the generation of Mg-Al-Ni ternary phase in the FZ.

3.4 Bonding Mechanism

Based on the microstructure analyses and the results of thermodynamic calculation, the bonding mechanism was illuminated. The schematic of joining process of Mg/Ti with the Ni coating is shown in Fig. 8. During laser heating process, AZ92 Mg-based filler metal melted firstly and dropped down, while the molten Ni coating wetted the surface of Ti sheet and contributed to the spreading of molten Mg filler. At the groove, the molten Ni coating diffused to fusion zone and Ti substrate, which promoted the interfacial reaction.

The atoms diffusion tendency above 1180 °C is shown in Fig. 8(b). According to the thermodynamic calculation, Ni atoms and Al atoms diffused from fusion zone to Ti substrate and mixed with the Ti atoms with different degrees of activation, because the temperature of joints decreased from bottom zone to top zone. Combined with chemical potential, Al atoms showed a faster diffusion tendency than Ni atoms. When the temperature decreased below 1180 °C, Ti_3Al phase precip-

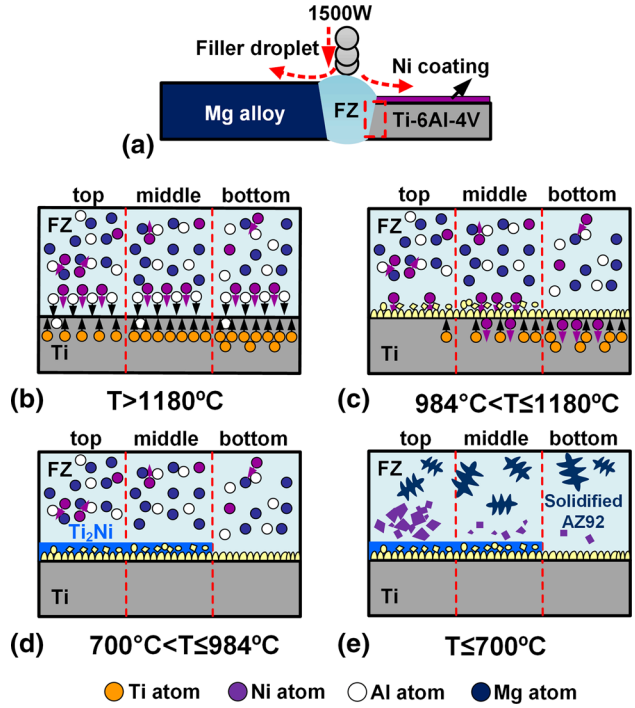

Fig. 8 Schematic of bonding mechanism: (a) laser irradiation; (b) the atoms diffusion tendency above 1180 °C; (c) Ti_3Al phase precipitated at FZ/Ti interface; (d) Ti_2Ni phase precipitated around Ti_3Al phase; (e) Mg_3AlNi_2 and $Mg_{17}Al_{12}$ were precipitated in the FZ

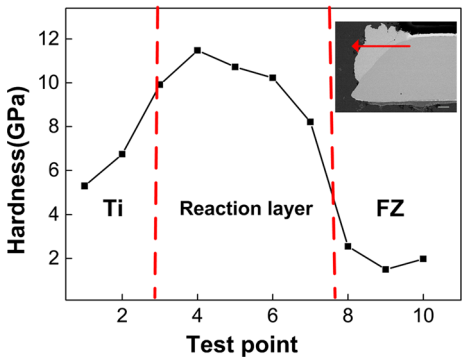

Fig. 9 The results of nanoindentation test with 5.8 μm coating thickness

itated firstly at FZ/Ti interface shown in Fig. 8(c). As the temperature decreased from 1180 to 984 °C, Ni continued to diffuse surrounding Ti substrate and Ti_3Al phase. Then Ti_2Ni phase precipitated around Ti_3Al phase at 984 °C or below.

As temperature continuously decreased, Mg, Al and Ni atoms assembled in the fusion zone and Mg_3AlNi_2 were produced at 700 °C because of the driving force of Gibbs free energy. Finally, the molten AZ92 filler began to solidify at 650 °C and the second phase $Mg_{17}Al_{12}$ was precipitated in the FZ when the temperature dropped down to 327 °C, as shown in Fig. 8(e).

3.5 Mechanical Properties

The nanoindentation test was operated along the interfacial layer of the top region of the Mg/Ti joint. The maximum depth

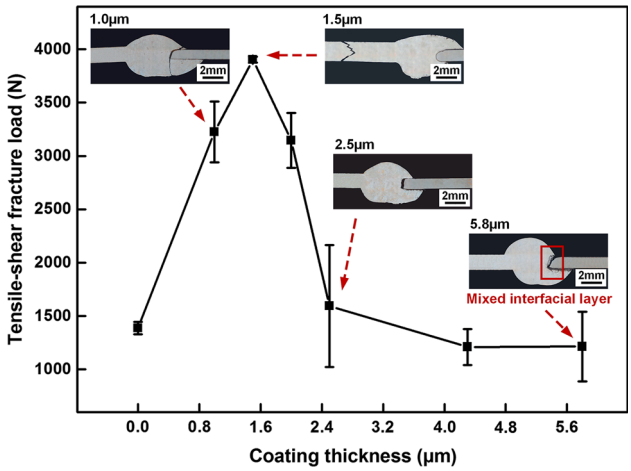

Fig. 10 Tensile shear fracture load vs. Ni coating thickness

of penetration was 300 nm and Poisson ratio was 0.25. As shown in Fig. 9, nanoindentation started at the Ti matrix, propagated through the reaction layer and finished in the FZ. The interval of adjacent indentation was 30 μm. The hardness of reaction layer was higher than that of Ti and FZ, which was attributed to a large amount of Ni atoms diffused to activated Ti and then formed Ti_2Ni intermetallics.

Tensile shear testing was carried out to evaluate the fracture loads of Mg-/Ni-coated Ti joints with different coating thicknesses and the results are plotted in Fig. 10. Interfacial failure occurred in the non-coated Mg/Ti joint, with fracture load of 1378 N. The fracture load then increased with the increase in Ni coating thickness and the highest value of 3900 N was obtained at thickness of 1.5 μm. In this case, the fracture location was changed to Mg base metal. Two main reasons were responsible for this enhancement. The wetting and spreading ability of molten Mg filler on Ti was improved with thicker Ni coating causing more coverage of filler on Ti surface, which increased fracture load. In addition, newly formed Ti_2Ni+Ti_3Al mixed interfacial layer enhanced metallurgical joining between Mg and Ti. Thus, the Mg/Ti interface was not the weakest region of the joint after adding coating layer. The tensile shear force dropped with further increase in coating thickness. The cracks and slag inclusions (Fig. 4(c1) and (d1)-(d3)) produced in thick interfacial reaction layer gave rise to this phenomenon. Based on the fracture path inserted in Fig. 10, crack propagated mainly through the mixed reaction layer and surface of Ti substrate. The fluctuation of tensile shear force suggested that the control of interfacial reaction layer was the key to excellent joint performance, which further suggested that the interlayer thickness played an important role in metallurgical reaction and interfacial layer thickness.

Figure 11 exhibits the fracture surface morphologies of Mg/Ti joint with different Ni coating thickness. All SEM micrographs were obtained from the Ti side. The relevant EDS analysis result of typical phase is listed in Table 5. For Mg-/Ni-coated Ti joint with 1-μm-thick coating, fracture surface was characterized by the tear ridges and terraces as shown in Fig. 11(a), indicating severe deformation generated in the process of tensile shear test. Higher magnification of zone b is presented in Fig. 11(b). Banded structure P1 and some white phases P2 were observed on the matrix P3. According to the EDS result, P1 was composed of 88.26 at.% Mg, 8.51 at.% Al

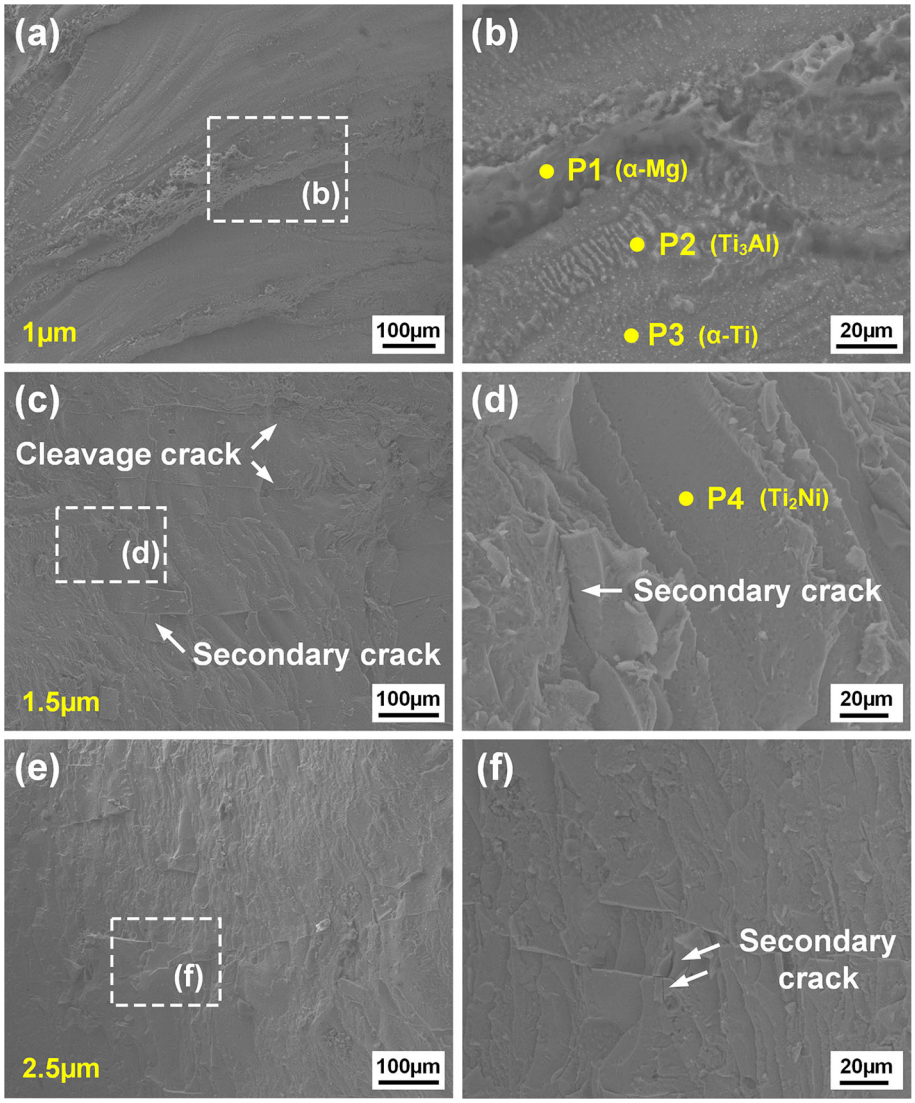

Fig. 11 Fracture surface morphologies at Ti side with various Ni coating thickness: (a) 1 μm; (b) higher magnification of Zone b; (c) 2.5 μm; (d) higher magnification of Zone d; (e) 5.8 μm; (f) higher magnification of Zone f

Table 5 Component of different points in Fig. 10 (at.%)

Point	Mg	Al	Ti	Ni	Possible phase
P1	88.26	8.51	2.39		$Mg_{17}Al_{12}$
P2	17.20	22.30	60.50		Ti_3Al
P3	11.11	13.44	75.45		α-Ti
P4	0.18	8.66	60.92	30.24	Ti_2Ni

and 2.39 at.% Ti, indicating some residual α-Mg was attached at fracture surface of Ti side. The phase P2 was identified as Ti_3Al because it mainly contained 22.30 at.% Al and 60.50 at.% Ti, which was in accordance with the confirmation of interfacial layer as shown in Fig. 4(a1)-(a3) and 5(a). The dark matrix P3 consisted of 11.11 at.% Mg, 13.44 at.% Al and 75.45 at.% Ti, implying it was α-Ti. The residual $Mg_{17}Al_{12}$ and Ti_3Al suggested that metallurgical joining was realized and this Ti-Al compound could improve the bonding between Mg and Ti alloy. With the increasing Ni coating thickness, fracture was cleavage fracture which was characterized by river pattern as presented in Fig 11(c)-(f).

Some secondary cracks were observed in vertical direction of cleavage crack. The EDS analysis result confirmed P4 was Ti_2Ni primarily containing 60.92 at.% Ti and 30.24 at.% Ni. This result agreed with the observation of Fig. 4(c1), (d2) and (d3), which was further evidence that thick interfacial reaction layer was detrimental to joint strength.

4. Conclusions

Laser welding–brazing of Mg to Ni-coated Ti in butt configuration with AZ92 Mg-based filler was investigated. The effect of electroplated interlayer thickness on microstructure and mechanical properties was studied. The bonding mechanism was illuminated according to the analysis results above. The main conclusions were as follows:

(1) Uniform appearances of Mg/Ti joints were achieved with Ni electroplated coating. The contact angles exhibited decrease trend first and then kept constant as coating thickness increased from 1 to 5.8 μm.
(2) Only Ti_3Al interfacial reaction layer formed when using 1-μm coating. Ti_2Ni+Ti_3Al mixed layer was produced as coating thickness excessed 1.5 μm. Slag inclusion and crack occurred with further increase in Ni coating. The thickness of interfacial layer at the top groove was thicker than that at the bottom groove of the same joint. The similar phenomenon of Mg-Al-Ni ternary phase in the FZ was observed.
(3) The thermodynamic calculation results of chemical potential indicated that Al atoms diffused faster than Ni in fusion zone. Mg-Al-Ni ternary phase, Al-Ti and Ni-Ti binary phases were generated spontaneously owing to the decreased Gibbs free energy.
(4) The maximum fracture load was 3900 N with the Ni coating thickness of 1.5 μm when joint fractured at the Mg base metal. Insufficient interfacial reaction or excessive intermetallic compound product along the interface caused interfacial failure.

Acknowledgments

The study was financially supported by National Natural Science Foundation of China (Grant No. 51875129), Key Research & Development Program in Shandong Province (Grant Nos. 2017GGX30147 and 2017CXGC0811), China, and Postdoctoral Science Foundation (Grant No. 2016T90280).

References

1. W.M. Elthalabawy and T.I. Khan, Microstructural Development of Diffusion-Brazed Austenitic Stainless Steel to Magnesium Alloy Using a Nickel Interlayer, *Mater. Charact.*, 2010, **61**(7), p 703–712
2. L. Zhou, Z.Y. Li, X.G. Song, C.W. Tan, Z.Z. He, Y.X. Huang, and J.C. Feng, Influence of Laser Offset on Laser Welding-Brazing of Al/Brass Dissimilar Alloys, *J. Alloys Compd.*, 2017, **717**, p 78–92
3. A. Abdollah-Zadeh, T. Saeid, and B. Sazgari, Microstructural and Mechanical Properties of Friction Stir Welded Aluminum/Copper Lap Joints, *J. Alloys Compd.*, 2008, **460**(1–2), p 535–538
4. S. Chen, D. Yang, J. Yang, J. Huang, and X. Zhao, Nanoscale Structures of the Interfacial Reaction Layers Between Molten Aluminium and Solid Steel Based on Thermophysical Simulations, *J. Alloys Compd.*, 2018, **739**, p 184–189
5. H.T. Zhang, J.C. Feng, P. He, B.B. Zhang, J.M. Chen, and L. Wang, The Arc Characteristics and Metal Transfer Behaviour of Cold Metal Transfer and its Use in Joining Aluminium to Zinc-Coated Steel, *Mater. Sci. Eng. A*, 2009, **499**(1), p 111–113
6. T. Tanaka, N.A. Gokcen, and Z.I. Morita, Relationship Between Partial Enthalpy of Mixing and Partial Excess Entropy of Solute Elements in Infinitely Dilute Solutions of Liquid Binary Alloys, *Z. Metall.*, 2013, **81**(5), p 349–353
7. G. Casalino, P. Guglielmi, V.D. Lorusso, M. Mortello, P. Peyre, and D. Sorgente, Laser Offset Welding of AZ31B Magnesium Alloy to 316 Stainless Steel, *J. Mater. Process. Technol.*, 2017, **242**, p 49–59
8. S. Chen, L. Li, Y. Chen, and J. Huang, Joining Mechanism of Ti/Al Dissimilar Alloys During Laser Welding-Brazing Process, *J. Alloys Compd.*, 2011, **509**(3), p 891–898
9. G. Casalino, M. Mortello, and P. Peyre, Yb–YAG Laser Offset Welding of AA5754 and T40 Butt Joint, *J. Mater. Process. Technol.*, 2015, **223**, p 139–149
10. G. Casalino and M. Mortello, Modeling and Experimental Analysis of Fiber Laser Offset Welding of Al-Ti Butt Joints, *Int. J. Adv. Manuf. Technol.*, 2016, **83**(1–4), p 89–98
11. L. Liu and H. Wang, Microstructure and Properties Analysis of Laser Welding and Laser Weld Bonding Mg to Al Joints, *Metall. Mater. Trans. A*, 2011, **42**(4), p 1044–1050
12. M.K. Kulekci, Magnesium and its Alloys Applications in Automotive Industry, *Int. J. Adv. Manuf. Technol.*, 2008, **39**(9–10), p 851–865
13. H.E. Friedrich and B.L. Mordike, *Magnesium Technology—Metallurgy, Design Data, Application*, DLR, Stuttgart, 2006
14. M. Peters, J. Hemptenmacher, J. Kumpfert, and C. Leyens, *Structure and Properties of Titanium and Titanium Alloys*, Wiley-VCH Verlag GmbH & Co. KGaA, New York, 2003
15. E. Akman, A. Demir, T. Canel, and T. Sınmazçelik, Laser Welding of Ti6Al4V Titanium Alloys, *J. Mater. Process. Tech*, 2009, **209**(8), p 3705–3713
16. M. Aonuma and K. Nakata, Effect of Alloying Elements on Interface Microstructure of Mg–Al–Zn Magnesium Alloys and Titanium Joint by Friction Stir Welding, *Mater. Sci. Eng., B*, 2009, **161**(1–3), p 46–49
17. M. Gao, Z.M. Wang, X.Y. Li, and X.Y. Zeng, Laser Keyhole Welding of Dissimilar Ti-6Al-4V Titanium Alloy to AZ31B Magnesium Alloy, *Metall. Mater. Trans. A*, 2012, **43**(1), p 163–172
18. R. Cao, T. Wang, C. Wang, Z. Feng, Q. Lin, and J.H. Chen, Cold Metal Transfer Welding–Brazing of Pure Titanium TA2 to Magnesium Alloy AZ31B, *J. Alloys Compd.*, 2014, **605**(14), p 12–20
19. C. Tan, X. Song, B. Chen, L. Li, and J. Feng, Enhanced Interfacial Reaction and Mechanical Properties of Laser Welded-Brazed Mg/Ti Joints with Al Element from Filler, *Mater. Lett.*, 2016, **167**, p 38–42
20. A.M. Atieh and T.I. Khan, Effect of Process Parameters on Semi-solid TLP Bonding of Ti–6Al–4V to Mg–AZ31, *J. Mater. Sci.*, 2013, **48**(19), p 6737–6745
21. C. Zang, J. Liu, C. Tan, K. Zhang, X. Song, B. Chen, L. Li, and J. Feng, Laser Conduction Welding Characteristics of Dissimilar Metals Mg/Ti with Al Interlayer, *J. Manuf. Process.*, 2018, **32**, p 595–605
22. C. Tan, X. Gong, L. Li, and J. Feng, Laser Welding-Brazing Characteristics of Dissimilar Metals Mg/Ti with Al Interlayers, *Chin. J. Lasers*, 2015, **42**(1), p 0103002-0103001–0103002-0103008
23. Z. Zhang, C. Tan, G. Wang, B. Chen, X. Song, H. Zhao, L. Li, and J. Feng, Laser Welding-Brazing of Immiscible AZ31B Mg and Ti-6Al-4V Alloys Using an Electrodeposited Cu Interlayer, *J. Mater. Eng. Perform.*, 2018, **27**(3), p 1414–1426
24. C. Tan, J. Yang, X. Zhao, K. Zhang, X. Song, B. Chen, L. Li, and J. Feng, Influence of Ni Coating on Interfacial Reactions and Mechanical Properties in Laser Welding-Brazing of Mg/Ti Butt Joint, *J. Alloys Compd.*, 2018, **764**, p 186–201
25. C. Tan, Q. Lu, B. Chen, X. Song, L. Li, J. Feng, and Y. Wang, Influence of Laser Power on Microstructure and Mechanical Properties of Laser Welded-Brazed Mg to Ni Coated Ti Alloys, *Opt. Laser Technol.*, 2017, **89**, p 156–167
26. A.R. Miedema, P.F.D. Châtel, and F.R.D. Boer, Cohesion in Alloys—Fundamentals of a Semi-empirical Model, *Physica B+c*, 1980, **100**(1), p 1–28
27. L. Li, H. Xia, C. Tan, and N. Ma, Effect of Groove Shape on Laser Welding-Brazing Al to Steel, *J. Mater. Process. Technol.*, 2018, **252**, p 573–581